Electrochemical Lithium Doping of Cu2-xS Nanocrystal Assemblies for Tuning Their Near Infrared Absorbance

Electrochemical Lithium Doping of Cu$_{2-x}$S Nanocrystal Assemblies for Tuning Their Near Infrared Absorbance

HanKyul Lee,[a, #] Hyunwoo Jo,[a, #] Jong Ik Lee,[a] Agni Raj Koirala,[b] Hwichan Cho,[a] Wansoo Huh,[c]

and Moon Sung Kang[*ad]

[a] Department of Chemical and Biomolecular Engineering, Sogang University, Seoul 04107,

Korea

[b] Department of Chemical Engineering, Soongsil University, Seoul 06978, Korea;

[c] Department of Chemistry, Korea Center for Artificial Photosynthesis (KCAP), Sogang

University, Seoul 04107, Korea

[d] Institute of Emergent Materials, Sogang University, Seoul 04107, Korea

[#] These authors contributed equally to this work

* Corresponding author. Email address: kangms@sogang.ac.kr (Moon Sung Kang)

ABSTRACT

The charge carrier density of copper sulfide nanocrystals ($Cu_{2-x}S$ NCs) is sensitive to variations in the atomic composition, which determines the nature of sulfur bonding (sulfur-to-sulfur bonding or copper-to-sulfur bonding) in the lattice. Therefore, the fine control of the composition of $Cu_{2-x}S$ NCs, particularly in thin-film assemblies, provides a versatile strategy for tuning the electronic properties of materials that can be directly applied in electronic devices. Herein, we report that the atomic composition of the $Cu_{2-x}S$ NC assemblies ($x = 0.9$; cation/anion ratio = 1.1/1) can be controlled by introducing monovalent lithium ions into the assemblies (yielding $Li_{0.7}Cu_{2-x}S$ NCs; $x = 0.9$; cation/anion ratio = 1.8/1) and reversibly extracting these cations from the assemblies through electrochemical methods. The electrochemically controlled uptake and release of lithium ions in $Cu_{2-x}S$ NC assemblies enabled the systematic tuning of the characteristic near-infrared absorbance (NIR) of the thin-film assemblies based on the localized surface plasmon resonance; NIR absorbance at 1300 nm wavelength, for example, could be controlled by larger than 75% by exploiting the reversible doping process.

Keywords: lithiation, copper sulfide nanocrystal, nanocrystal assembly, doping

Introduction

Variation in the atomic stoichiometry of copper sulfide nanocrystals ($Cu_{2-x}S$ NCs, where x represents the degree of mismatched stoichiometry between copper and sulfur and has a range from 0 to 1) leads to the materials with diverse crystal structure phases.[1-3] This is possible because of the versatility of sulfur bonding.[4] Sulfur in copper-to-sulfur bonds, which are referred to as monosulfide bonds and are abundant in $Cu_{2-x}S$ NC under copper-rich conditions (i.e., smaller x), can form sulfur-to-sulfur bonds, which are referred to as disulfide bonds, under copper-deficient conditions (i.e., larger x), leading to the p-type self-doping of the lattice. Therefore, the hole density and the associated electronic properties of $Cu_{2-x}S$ NCs in thin-film assemblies can be tuned by delicately controlling the atomic stoichiometry.[5, 6] These properties include characteristic absorbance in the near-infrared (NIR) region based on localized surface plasmon resonance (LSPR), thermoelectrical conductivity, and electrical conductivity, which can be separately and collectively exploited in next-generation optoelectronic and energy devices.[7-17]

A promising strategy to alter the atomic stoichiometry of $Cu_{2-x}S$ NCs is to vary the ratio of copper and sulfur precursors[18-21] or to control the reactivity of these precursors by manipulating the surface ligands that are dynamically absorbed on the crystal surface during growth.[22-26] Although this method is simple, acquiring the on-demand control of the atomic stoichiometry in this method is challenging, owing to the experimental uncertainties that occur during crystal growth. The atomic stoichiometry of $Cu_{2-x}S$ NCs can also be controlled by post-treatment after the synthesis or even after the NC thin-film deposition. Furthermore, the ligand removal/exchange process for enhancing electronic coupling between NCs can be conducted prior to the post-treatment, which is critical for exploiting the materials for thin-film optoelectric devices.[27] For example, Lee et al.[28] demonstrated that the LSPR properties or

thermoelectric/electric properties of $Cu_{2-x}S$ NC assemblies can be tuned using a chemical agent that either provides Cu^+ to the lattice (e.g., tetrakis copper hexafluorophosphate, $[Cu(CH_3CN)_4]PF_6$) or extracts Cu^+ from the lattice (e.g., cerium ammonium nitrate, $(NH_4)_2[Ce(NO_3)_6]$). By changing the duration of the chemical post-treatment, the physical properties of the $Cu_{2-x}S$ NC assemblies, including their LSPR characteristics, could be varied systematically with the contents of Cu^+. A series of samples can be easily prepared using this chemical method by gradually varying atomic stoichiometries, which is beneficial for a systematic study. However, because of its reliance on the control of the reaction time, this method cannot be employed for the on-demand control of the atomic stoichiometry of $Cu_{2-x}S$ NCs with minimal batch-to-batch error. For practical applications of the characteristic LSPR effect of $Cu_{2-x}S$ NCs in NIR optical device applications, the optical properties of the materials, especially in their closely packed thin film assemblies, should be controlled using an electrical source in a reversible manner.

Herein, we report the tuning of the atomic stoichiometry of $Cu_{2-x}S$ NC assemblies using lithium ions through electrochemical methods. Electrochemical methods based on applied-potential-dependent electrochemical reactions allow the reversible control of the ion-insertion/extraction reactions in $Cu_{2-x}S$ NC assemblies. We observed that the characteristic LSPR in the NIR region of the $Cu_{2-x}S$ NC assemblies could be suppressed based on the induced electrochemical reaction when a negative potential is applied to the assemblies, indicating that the density of hole carriers in the assemblies could be controlled. Meanwhile, the reverse reaction induced under a positive potential increased the hole density in the assemblies and amplified the LSPR.

Experimental methods

Chemicals and materials

Copper(I) chloride (99.995%), sulfur powder (99.98%), oleylamine (OAm, technical grade, 70%), sodium sulfide (Na_2S), hexane (anhydrous, 95%), toluene (anhydrous, 99.8%), ethanol (anhydrous, ≥99.5%), chloroform (anhydrous, ≥99%), propylene carbonate (PC, anhydrous, 99.7%), dimethyl carbonate (anhydrous, ≥99%), tetrabutylammonium perchlorate (TBAP, ≥95%), ferrocene (Fc; 98%), and lithium perchlorate (99.99%)were purchased from Sigma-Aldrich. The chemicals were used as received without further purification. Indium tin oxide (ITO)-coated glass substrates were purchased from AMG (Korea). The electrodes used for the electrochemical cells were purchased from CorrTest Instruments.

Synthesis of $Cu_{1.1}S$ NCs

$Cu_{1.1}S$ NCs were synthesized by modifying a previously described method.[3, 28] Copper(I) chloride (118.8 mg) was added to OAm (24 mL) in a three-neck round-bottom flask followed by degassing to form a copper precursor solution. Separately, sulfur powder (48.1 mg) was added to OAm (15 mL) in a three-neck round-bottom flask and degassed to form a sulfur precursor solution. The flask containing the sulfur precursor solution was heated at 120 °C for 25 min under a nitrogen atmosphere and then cooled to 40 °C. Meanwhile, the reaction flask with copper(I) chloride was heated at 225 °C under a nitrogen atmosphere until the solution became transparent and then cooled to 125 °C. Subsequently, the sulfur precursor solution (12 mL, 40 °C) was swiftly injected into the reaction flask at 125 °C, and the temperature was maintained at 104 °C for 90 s to allow $Cu_{1.1}S$ NC growth. The temperature was then rapidly reduced to room temperature. The resulting NC solution was purified by centrifuging the reaction mixture using

ethanol and a 3:7 mixture of hexane and toluene as the anti-solvent and solvent, respectively, for

the dispersion.

Preparation of electrically coupled assemblies of Cu$_{1.1}$S NCs

The glass substrate and pre-coated ITO electrodes were sequentially cleaned via sonication in

acetone and isopropanol. Dispersions of the Cu$_{1.1}$S NCs (20 mg mL^{-1}) in a hexane:toluene

solution (3:7 volume ratio) were spin-coated (2500 rpm, 60 s) onto the substrates, and the

resulting films were annealed at 65 °C for 30 min. Na$_2$S in ethanol (0.064 M) was dropped onto

the Cu$_{1.1}$S NC film, dwelled for 2 min, and spin-coated at 2500 rpm for 15 s. This dwelling time

was sufficient to completely remove the original OAm ligands on the surface of the Cu$_{1.1}$S NCs.

The resulting films were rinsed with fresh ethanol and heated at 80 °C for 3 min on a hot plate.

The thin-film formation and ligand removal processes were repeated to form fully percolated,

electronically coupled assemblies of Cu$_{1.1}$S NCs.

**Electrochemical insertion/extraction of lithium ions into electronically coupled assemblies
of Cu$_{1.1}$S NCs**

A three-electrode electrochemical system was used in this study. Assemblies of Cu$_{1.1}$S NCs

deposited onto ITO surfaces were used as the working electrode; a Pt wire was used as the

counter electrode, and a Ag wire was used as the reference electrode. As the electrolyte solution,

100 mM lithium perchlorate, 100 mM TBAP, and 1 mM Fc were dissolved in PC. For X-ray

photoemission spectroscopy (XPS) measurements, the Cu$_{1.1}$S NC assemblies were rinsed with

fresh dimethyl carbonate to remove any residual PC.

Characterization of assemblies of Cu$_{1.1}$S NCs

Transmission electron microscopy (TEM) was performed using a Libra 120 (Carl Zeiss)

instrument operating at 120 keV. Ultraviolet (UV)-visible (Vis)-NIR spectra were obtained using

a V-770 UV-Vis/NIR spectrophotometer (Jasco). XPS measurements were conducted using an

AXIS Ultra DLD instrument (Kratos). Fourier transform infrared (FT-IR) spectra were obtained

using an FT-IR 4700 spectrometer (Jasco). Atomic force microscopy (AFM) measurements were

performed using a Park XE7 instrument (Park Systems).

Results and discussion

The $Cu_{2-x}S$ NCs used in this study were synthesized using a hot-injection method based on a

modified protocol described previously (Step 1).[28] Copper(I) chloride and sulfur powder were

used as the copper and sulfur precursors, respectively. OAm was used as the reaction solvent as

well as the ligands attached to the NC surface. The average diameter of the as-synthesized $Cu_{2-x}S$

NCs capped with OAm is 5.5. An x-value of 0.9 was confirmed for these NCs based on the

composition analysis using XPS. Fig. 1b shows the UV-Vis-NIR spectrum of the resulting $Cu_{1.1}S$

NCs dispersed in trichloroethylene. The LSPR peak appearing at ~1400 nm in the NIR region

indicates abundant holes in the $Cu_{1.1}S$ NCs created because of the stoichiometry-dependent self-

doping.[29] The X-ray diffraction (XRD) pattern of the as-synthesized $Cu_{1.1}S$ NCs matches that

reported for $Cu_{1.3}S$ NCs by Manna et al.[4] or $Cu_{1.1}S$ NCs by Kang et al.,[28] which is ascribed to a

set of peaks negatively shifted from the covellite phase (CuS) (Fig. 1c). In addition, the Scherrer

equation was applied to the broadening of the peak at 42.6°, which yielded the size of the $Cu_{1.1}S$

NCs to be 5.1 nm. This is consistent with the NC size obtained from TEM analysis. The $Cu_{1.1}S$

NCs are assembled onto a glass substrate coated with an ITO layer (Step 2, Fig. 1d). The

morphology of the film was analyzed using AFM, and the results are shown in Fig. 1e. The root

mean square (RMS) roughness of the surface is 0.8 nm. Despite the reduced average NC–NC

distance in the assemblies compared to that in solution, the thin film shows a characteristic LSPR

peak at ~1100 nm in the NIR region (Fig. 1f).
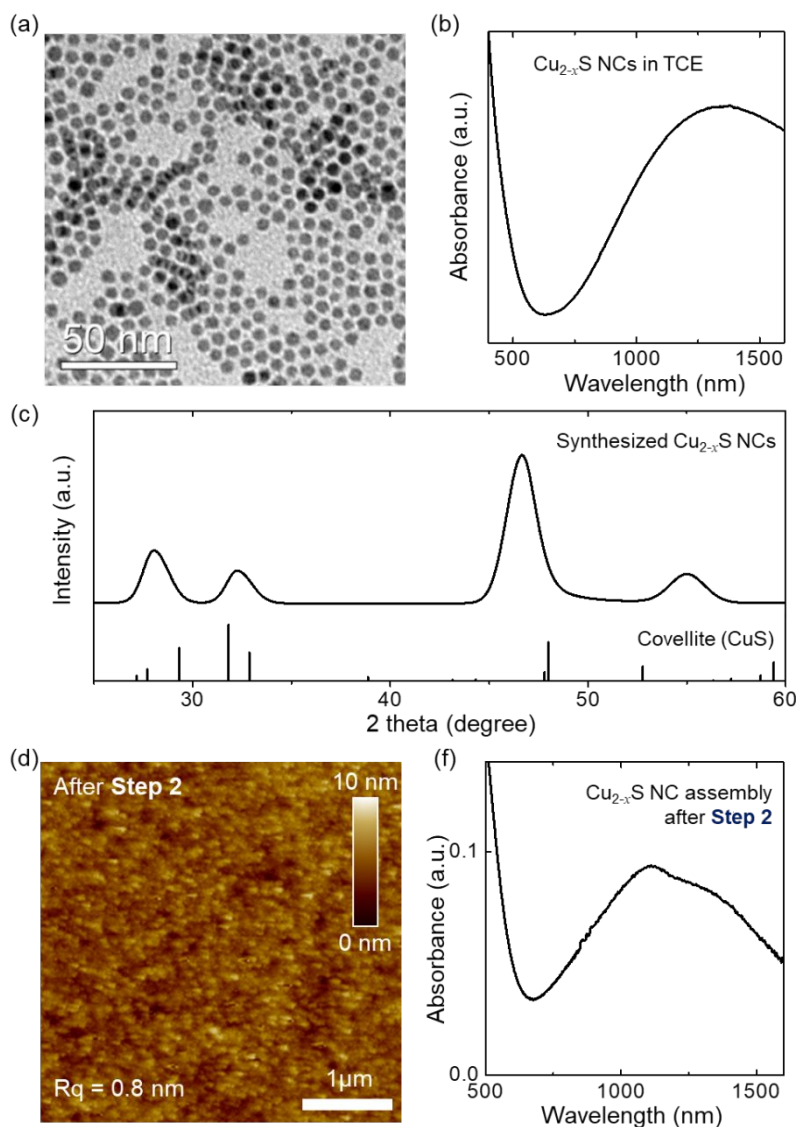
Fig. 1 (a) A TEM image of the $Cu_{2-x}S$ NCs ($x = 0.9$). (b) UV-Vis-NIR absorbance spectrum of the $Cu_{2-x}S$ NCs in solution (trichloroethylene). (c) X-ray diffractogram of $Cu_{2-x}S$ NCs. A set of peaks for covellite phase is also drawn. The negative shift of the peaks for $Cu_{2-x}S$ NCs relative to the covellite reference can be ascribed to the role of excessive Cu intercalating the covellite lattice for $Cu_{2-x}S$ NCs.[4] (d) AFM image of the resulting $Cu_{2-x}S$ NC assembly (film thickness = 23 nm). (f) UV-Vis-NIR absorbance spectrum of the $Cu_{2-x}S$ NC assembly.

Subsequently, the OAm ligands on the surface of the $Cu_{1.1}S$ NCs were removed via Na_2S treatment (Step 3, Fig. 2a). Based on our previous study,[28] dipping thin films of $Cu_{2-x}S$ NCs into a Na_2S solution in methanol completely removed the OAm without altering the composition of the $Cu_{2-x}S$ NCs. Adding a drop of Na_2S solution (0.064 M in ethanol) onto the $Cu_{1.1}S$ NC assemblies and dwelling for 2 min followed by the spin-drying of the samples yielded consistent results. Fig. 2b shows the FT-IR spectra of the $Cu_{1.1}S$ NC assemblies before and after the Na_2S treatment. The peak at approximately 2800–3000 cm^{-1} assigned to the stretching vibration of the C-H bond of OAm is completely eliminated after the Na_2S treatment step. The removal of the insulating OAm from the surface of the NCs enhances the electronic coupling between neighboring NCs and increases the conductivity of the assemblies.[30-33] Additionally, OAm removal facilitated an easier access of ions (such as lithium ions) in the electrochemical cells during electric-potential-dependent electrochemical reactions. Because ligand removal often produced microscopic cracks in the film, we repeatedly performed the aforementioned spin-coating of NCs and ligand removal steps to fill the cracks while preserving good coupling between neighboring NCs. Fig. 2c shows the morphology of the resulting highly coupled $Cu_{1.1}S$ NC assemblies as observed using AFM. No distinct cracks or pinholes are observed. The RMS roughness of the film was 1.7 nm, indicating that repeated NC casting and ligand removal steps gently increased the surface roughness. The UV-Vis-NIR absorbance spectrum of the resulting film is shown in Fig. 2d. Despite the enhanced coupling between the NCs due to the reduced average NC–NC distance after the Na_2S treatment, the assemblies exhibit a characteristic LSPR peak at ~1100 nm in the NIR region.
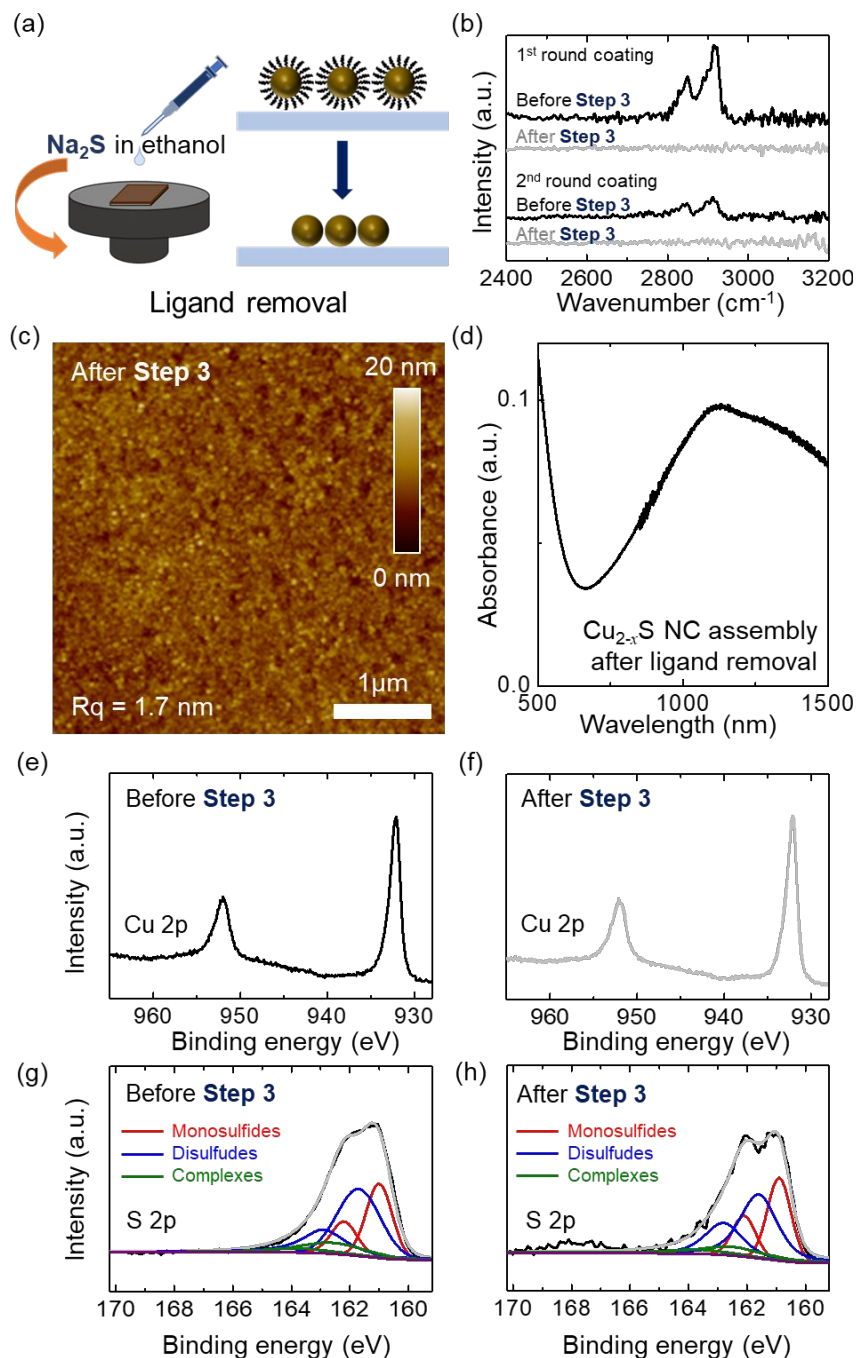
Fig. 2 (a) Schematic of the removal of ligands on the $Cu_{1.1}S$ NC assembly (Step 3). (b) FT-IR spectrum of $Cu_{1.1}S$ NC assemblies at different stages in Step 3. (c). AFM image of the $Cu_{1.1}S$ NC assembly after Step 3. (d) UV-Vis-NIR absorbance spectrum of the $Cu_{1.1}S$ NC assembly after Step 3. High-resolution Cu 2p XPS spectra of $Cu_{1.1}S$ NC assemblies before (e) and after (f) Step 3. High-resolution S 2p XPS spectra of $Cu_{1.1}S$ NC assemblies before (g) and after (h) Step 3. Deconvoluted subcomponents are colored to aid visualization.

The XPS elemental analysis confirms that Na_2S treatment and the associated ligand removal do not alter the atomic composition of the $Cu_{1.1}S$ NC assemblies (Table 1). Moreover, the analysis of high-resolution XPS profiles provided an in-depth understanding of the chemical states of the samples. Fig. 2e and f show the high-resolution XPS spectra of Cu 2p in the $Cu_{1.1}S$ NC assemblies before and after the Na_2S treatment, respectively. Two peaks at 932.1 and 952.0 eV are observed, corresponding to Cu $2p_{3/2}$ and Cu $2p_{1/2}$, respectively, and no noticeable differences are observed between the samples. The results indicate that the oxidation state of copper ($^+1$) is not altered during the ligand removal step. Fig. 2g and h show the high-resolution XPS spectra of S 2p in the $Cu_{1.1}S$ NC assemblies before and after the Na_2S treatment, respectively. As discussed above, sulfur bonding in the $Cu_{2-x}S$ NCs exists in two different forms: monosulfide bonding ($[S^{2-}]$) and disulfide bonding ($[(S-S)^-]$). Considering the charge neutrality, they can be expressed in a chemical formula as $Cu_{2-x}S = [Cu^+]_{2-x}[S^{2-}]_{1-2x/3}[(S-S)^-]_{x/3}$; for $Cu_{2-x}S$ NCs with $x = 0$ (i.e., $Cu_2S = [Cu^+]_2[S^{2-}]_1$), sulfur does not form disulfide boding. However, for $Cu_{2-x}S$ NCs with $x = 1$, (i.e., $CuS = [Cu^+]_1[S^{2-}]_{0.33}[(S-S)^-]_{0.33}$), two-thirds of the sulfur content contribute to form disulfide bonding. For the $Cu_{2-x}S$ NCs with $x = 0.9$, we expect the formula for $Cu_{1.1}S$ to be $[Cu^+]_{1.1}[S^{2-}]_{0.4}[(S-S)^-]_{0.3}$). The 4:3 ratio for $[S^{2-}]:[(S-S)^-]$ obtained using this formula matches well with the areal ratio of the respective deconvoluted peaks for the S 2p XPS spectrum. Notably, because two sulfur atoms are involved in a disulfide bond, the areal ratio between the monosulfide subcomponent peaks (at 160.9 and 162.1 eV) and disulfide subcomponent peaks (at 161.6 and 162.8 eV) corresponding to a 4:3 ratio for $[S^{2-}]:[(S-S)^-]$ should be 2:3. The areal ratio was 35.7:50.9 for the $Cu_{1.1}S$ NC assemblies before treatment with

Na_2S, and after the Na_2S treatment, the ratio was 36.1:50.1, indicating that the nature of the sulfur bonding in the $Cu_{1.1}S$ NC assemblies was not altered during the surface treatment.

Table 1 Chemical formula, degree of lithiation (y), areal ratio of the deconvoluted peaks of high-resolution S 2p spectra, and the binding energy of the S 2p for the $Cu_{2-x}S$ NC assemblies under different lithiation/delithiation conditions.

	Chemical Formula	y	Monosulfide content (%)	Disulfide content (%)	Complexes (%)	Monosulfide binding energy (eV)	Disulfide binding energy (eV)
Before ligand removal	$Cu_{1.1}S$	0	35.7	50.9	13.4	160.9 / 162.1	161.6 / 162.8
After ligand removal	$Cu_{1.1}S$	0	36.1	50.1	13.8	160.9 / 162.1	161.6 / 162.8
Lithiation (-0.9 V, 1 min)	$Li_{0.7}Cu_{1.1}S$	0.7	75.3	10.4	14.3	161.9 / 163.1	162.6 / 163.8
Delithiation (+0.9 V, 1 min)	$Li_{0.1}Cu_{1.1}S$	0.1	39.9	45.3	14.8	161.1 / 162.3	161.8 / 163.0

The resulting $Cu_{1.1}S$ NC assemblies formed on the ITO substrate served as the working electrode of an electrochemical cell that was used to conduct an electric-potential-controlled electrochemical reaction (e.g., a lithiation reaction) (Fig. 3a). For the electrochemical cell, we employed a silver (pseudo) reference electrode and a platinum counter electrode. PC combined with 100 mM TBAP was used as the electrolyte. Furthermore, 100 mM of lithium perchlorate was added to the electrolyte, which provided lithium ions for the lithiation reaction at the working electrode. Additionally, 1 mM of Fc was added to the electrolyte; the Fc/Fc^+ couple served as the redox mediator to facilitate the lithiation reaction at the working electrode.[34, 35]
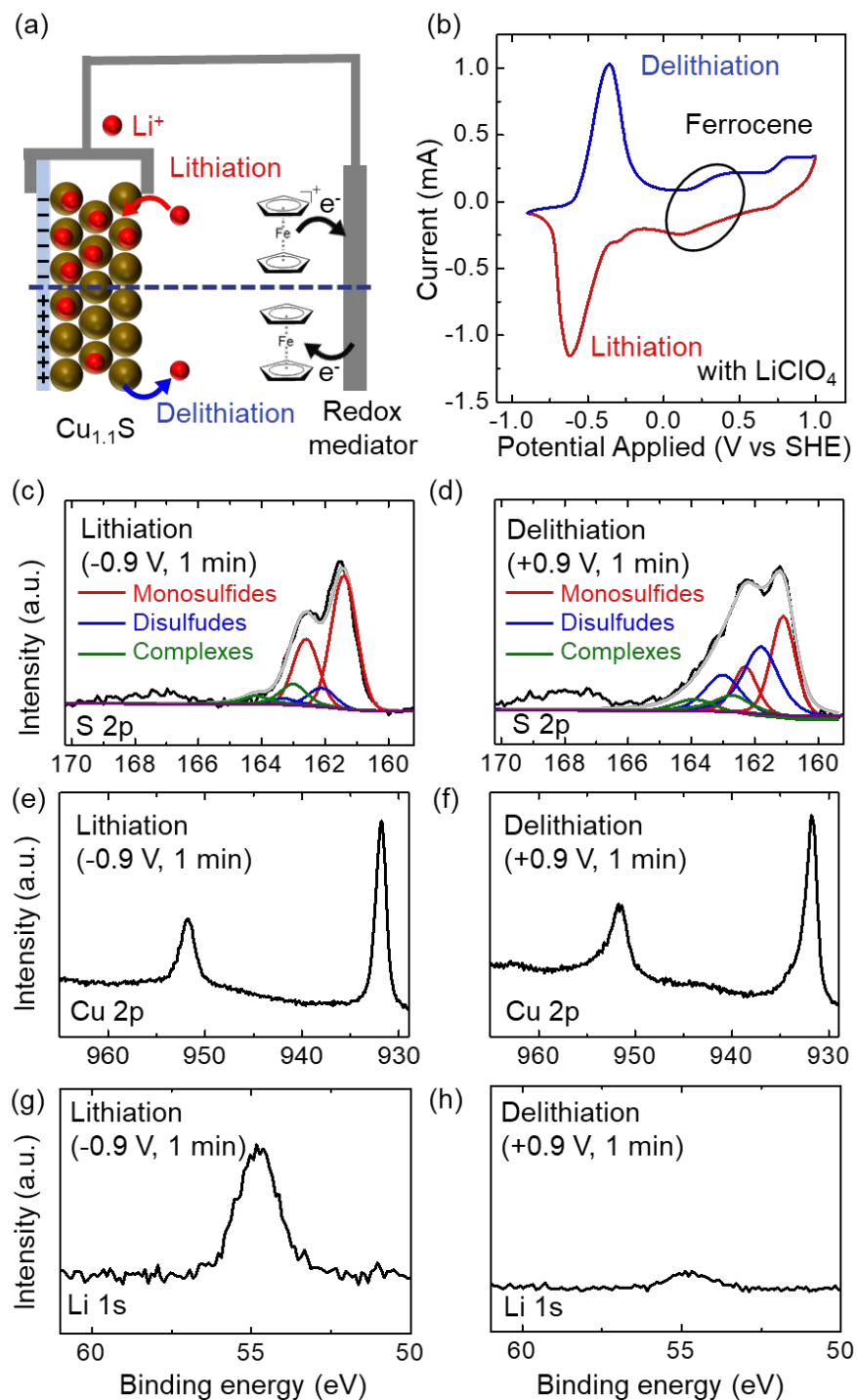
Fig. 3 (a) Schematic for the lithiation/delithiation process for the $Cu_{1.1}S$ NC assembly using the electrochemical method. (b) Cyclic voltammogram of the $Cu_{1.1}S$ NC assembly following the lithation/delithiation process. High-resolution S 2p (c, d), Cu 2p (e, f), and Li 1s (g, h) XPS spectra for the $Cu_{1.1}S$ NC assembly at different stages of the lithiation and delithiation processes.

We emphasize that exploiting lithium ions in the electrochemical cell is critical for the reversible control of the atomic composition of the $Cu_{2-x}S$ NC assemblies on the working electrode. Li^+ is monovalent. Therefore, the change in the lattice structure induced by Li^+ insertion/extraction is expected to occur as by the insertion/extraction of Cu^+ (for example, by the chemical treatment). Li^+ is stable in its monovalent form in electrolytic environments; therefore, it can be readily utilized in electrochemical cells. Notably, Cu^+ is likely to undergo a disproportionate reaction in an electrolytic environment ($2Cu^+ \rightarrow Cu^0 + Cu^{2+}$).[36, 37] Therefore, the utilization of Cu^+ in electrochemical cells requires the meticulous control of the electrolyte solution.[38, 39] In fact, the storage/release of Li^+ from $Cu_{2-x}S$ NCs has been intensively investigated for next-generation lithium ion-based energy storage devices.[10, 40, 41]

Fig. 3b shows a cyclic voltammogram of the as-prepared three-electrode electrochemical cell. A sharp reduction peak is observed at -0.6 V (relative to SHE), which is reversibly coupled to the oxidation peak at -0.4 V. The small peak at +0.4 V is ascribed to the half-wave potential of Fc.[42] We assign the reduction peak at -0.6 V observed during the forward scan to the lithiation reaction of the $Cu_{1.1}S$ NCs and the oxidation peak at -0.4 V detected during the reverse scan to the delithiation reaction.[10, 40, 41] When the $Cu_{1.1}S$ NCs are lithiated, the disulfide bonds break to form metal-sulfur bonds (i.e., monosulfide bonds), similar to the trend observed when additional Cu^+ is introduced into the NCs.[40, 41] We can express this phenomenon in a chemical equation as $y Li^+$ (from the electrolytic environment) $+ ye^-$ (from the Fc/Fc$^+$ couple) $+ Cu_{1.1}S$ ($= [Cu^+]_{1.1}[S^{2-}]_{0.40}[(S-S)^-]_{0.30}$) $\rightarrow Li_y Cu_{1.1}S$ ($= [Li^+]_y[Cu^+]_{1.1}[S^{2-}]_{0.40+2y/3}[(S-S)^-]_{0.30-y/3}$). Accordingly, we conjecture that the lithiation reaction induces a transformation in the bonding characteristics of sulfur such that additional monosulfide bonds are formed upon the insertion of the lithium ions.

This transformation is confirmed by the change in the shape of the S 2p XPS spectrum, which comprises subcomponents arising from monosulfides and disulfides. Fig. 3c and d show the high-resolution XPS profiles of S 2p for a $Cu_{1.1}S$ NC assembly under different lithiation/delithiation conditions. Fig. 3c shows the spectrum after applying -0.9 V (relative to SHE) to the $Cu_{1.1}S$ NC assembly for 1 min (the given lithiation condition yielded $Li_{0.7}Cu_{1.1}S$ NCs, the composition of which was determined via XPS elemental analysis), and Fig. 3d shows the results after applying +0.9 V (relative to SHE) for 1 min to the already lithiated $Cu_{1.1}S$ NC assembly (the given delithiation condition yielded $Li_{0.1}Cu_{1.1}S$ NCs, the composition of which was determined using the XPS elemental analysis). The areal ratio of the deconvoluted monosulfide and disulfide subcomponents for the S 2p XPS peak was 36.1:50.1 before lithiation (Fig. 2h). This ratio changed to 75.3:10.4 after lithiation, as the inserted lithium ions break the disulfide bonds and form monosulfide bonds. Finally, it changed to 39.9:45.3 after the delithiation process. Note that the original value (36.1:50.1) was not recovered. This is perhaps due to the residual lithium contained in the NC assembly even after the delithiation, which yielded the $Li_{0.1}Cu_{1.1}S$ NCs. In addition to the change in the peak intensities, a positive shift in the binding energy was observed for S 2p upon lithiation and vice versa upon delithiation. Consistent shift in the binding energy was also observed for $Cu_{2-x}S$ NCs that was inserted with Cu^+, which was attributed to the small change in Cu-S bond length upon insertion of additional cations.[4] The results are presented in Table 1.

The high-resolution XPS profiles of Cu 2p (e, f) and Li 1s (g, h) are also shown. For all the samples, the Cu 2p peaks appear at 932.1 and 952.0 eV and are assigned to the binding energies of $2p_{3/2}$ and $2p_{1/2}$ of Cu^+, respectively, indicating that copper exists in the +1 valency state during the entire experiment. Li peaks are not observed for the as-prepared $Cu_{1.1}S$ NC assembly.

However, after lithiation at -0.9 V (relative to SHE), the Li 1s peak is clearly observed. The intensity of this peak reduces after the as-lithiated $Cu_{1.1}S$ NC assembly is delithiated at +0.9 V (relative to SHE); however, it is not completely removed from the spectra as discussed above. Even after the application of the given delithiation potential over extended periods, the residual lithium component remained in the samples.

The lithiation process leading to changes in the characteristics of sulfur bonding is also expected to change the hole density of the $Cu_{2-x}S$ NC assembly, similar to the trend observed after inserting additional Cu^+ contents using chemical methods. The change in the hole density of the $Cu_{1.1}S$ NC assemblies was confirmed by monitoring the UV-Vis-NIR absorbance of the $Cu_{1.1}S$ NC assemblies while applying a potential to the assemblies using a spectroelectrochemical setup. As mentioned above, the characteristic NIR absorbance of the $Cu_{1.1}S$ NC assemblies is attributed to the LSPR, and the corresponding peak intensity is a sensitive function of the hole density of the materials. When a potential more negative than the peak reduction potential presented in Fig. 3b (i.e., -0.6 V relative to SHE) is applied (*e.g.*, -0.9 V) to the as-prepared $Cu_{1.1}S$ NC assembly, the LSPR absorbance peak intensity gradually decreases with time, indicating that its hole density is decreased (Fig. 4a). During the reverse scan of the cyclic voltammetry, when a potential more positive than the peak oxidation potential (-0.6 V relative to SHE) is applied (*e.g.*, +0.9 V) to the lithiated $Cu_{1.1}S$ NC assembly, the absorbance peak intensity in the NIR region gradually increases, indicating that its hole density is recovered (Fig. 4b). The lithiation and delithiation processes and the associated changes in LSPR were reversible and could be repeated multiple times (despite the residual amount of lithium remaining in the lattice, even after the delithiation). Fig. 4c shows the variation in the NIR absorbance at 1300 nm, as monitored by sweeping the potential applied to the $Cu_{1.1}S$ NC

16

assembly in cycles (the same as that of cyclic voltammetry). Along the lithiation and

deliathiation processes, the absorbance at this wavelength could be tuned by more than 75% of

its original value before the $Cu_{1.1}S$ NC assembly was lithiated. The change in the hole density of

the $Cu_{1.1}S$ NC assemblies could also be confirmed by analyzing the optical bandgap of the

material. As shown in Fig. 4d, e, lithiation systematically decreased the optical bandgap of $Cu_{2-x}S$ NC assemblies (from 3.10 to 3.02 eV), which could be recovered by delithiation (to 3.09 eV).

The change in the bandgap can be understood from the charge carrier density-dependent Moss-

Burstein effect, which has been widely observed for degenerate semiconductor systems.[43]
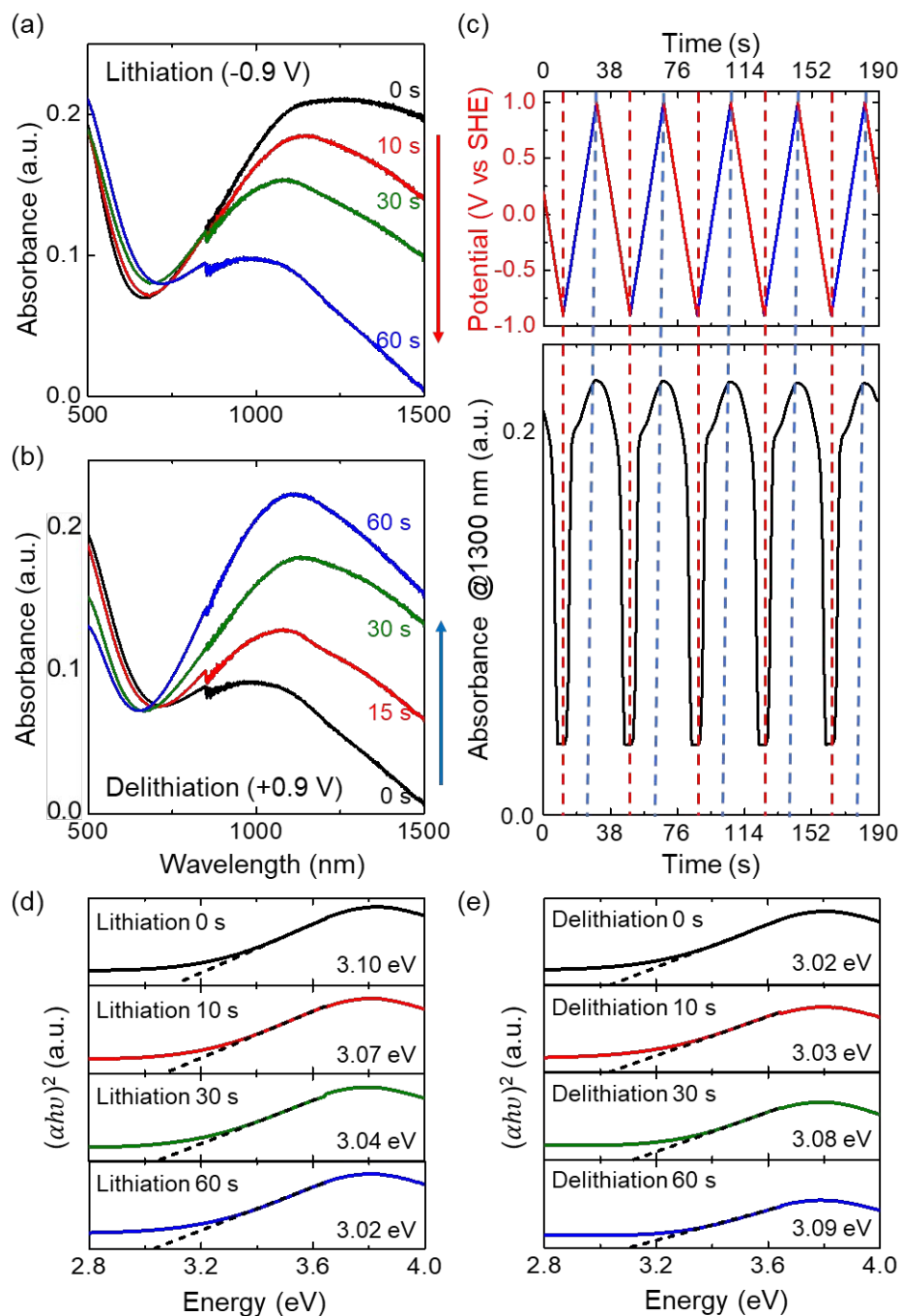
Fig. 4 Evolution of the absorbance spectrum during the (a) lithiation (V = -0.9 V relative to SHE) and (b) delithiation (V = +0.9 V relative to SHE) processes. (c) Absorbance monitored at 1300 nm with the application of cycling voltages between -0.9 and 1.0 V (scan rate = 100 mV/s). Tauc plots of the absorption spectra for $Cu_{2-x}S$ NCs assemblies during the (d) lithiation (V = -0.9 V relative to SHE) and (e) delithiation (V = +0.9 V relative to SHE) processes.

Conclusions

Here, we demonstrate that the doping characteristics of $Cu_{2-x}S$ NC assemblies, which in their pristine form are determined by the stoichiometric mismatch between copper and sulfur, can also be controlled by exploiting monovalent lithium ions through electrochemical methods. In particular, we confirmed that electrochemically introducing Li^+ to $Cu_{2-x}S$ NC assemblies yielded a consistent effect on the introduction of Cu^+ to the assemblies through chemical methods. Inserting Li^+ into the $Cu_{2-x}S$ NC assemblies at a negative potential systematically increased the formation of monosulfide bonds in the $Cu_{2-x}S$ lattice, decreased the hole density, and reduced the LSPR effects. The opposite effect was confirmed upon the application of a positive potential. Simple control on the optical response for thin-films assemblies of $Cu_{2-x}S$ NCs is expected to take a step closer to the realization of NIR electrochromic device applications. It would also provide a practical strategy to apply this material system in new, LSPR-based NIR optoelectronic systems, including sensors and optical filters. Moreover, this study contributes to the understanding of copper-chalcogenide-based ion-storage systems for energy device applications.

Conflicts of interest

There are no conflicts to declare.

Acknowledgements

References

1. C. Coughlan, M. Ibanez, O. Dobrozhan, A. Singh, A. Cabot and K. M. Ryan, *Chem. Rev.*, 2017, **117**, 5865-6109.

2. J. M. Luther, P. K. Jain, T. Ewers and A. P. Alivisatos, *Nat. Mater.*, 2011, **10**, 361-366.

3. X. Liu, X. Wang, B. Zhou, W. C. Law, A. N. Cartwright and M. T. Swihart, *Adv. Funct. Mater.*, 2013, **23**, 1256-1264.

4. Y. Xie, A. Riedinger, M. Prato, A. Casu, A. Genovese, P. Guardia, S. Sottini, C. Sangregorio, K. Miszta, S. Ghosh, T. Pellegrino and L. Manna, *J. Am. Chem. Soc.*, 2013, **135**, 17630-17637.

5. T. A. Patel and E. Panda, *Appl. Surf. Sci.*, 2019, **488**, 477-484.

6. Y. He, T. Day, T. Zhang, H. Liu, X. Shi, L. Chen and G. J. Snyder, *Adv. Mater.*, 2014, **26**, 3974-3978.

7. G. Kalimuldina, A. Nurpeissova, A. Adylkhanova, D. Adair, I. Taniguchi and Z. Bakenov, *ACS Appl. Energy Mater.*, 2020, **3**, 11480-11499.

8. Y. Wu, C. Wadia, W. Ma, B. Sadtler and A. P. Alivisatos, *Nano Lett.*, 2008, **8**, 2551-2555.

9. M. Basu, A. K. Sinha, M. Pradhan, S. Sarkar, Y. Negishi and T. Pal, *Environ. Sci. Technol.*, 2010, **44**, 6313-6318.

10. C.-H. Lai, K.-W. Huang, J.-H. Cheng, C.-Y. Lee, B.-J. Hwang and L.-J. Chen, *J. Mater. Chem.*, 2010, **20**, 6638-6645.

11. A. Šetkus, A. Galdikas, A. Mironas, I. Šimkiene, I. Ancutiene, V. Janickis, S. Kaciulis, G. Mattogno and G. Ingo, *Thin Solid Films*, 2001, **391**, 275-281.

12. M. Li, Y. Liu, Y. Zhang, X. Han, T. Zhang, Y. Zuo, C. Xie, K. Xiao, J. Arbiol and J. Llorca, *ACS Nano*, 2021, **15**, 4967-4978.

13. B. Jache, B. Mogwitz, F. Klein and P. Adelhelm, *J. Power Sources*, 2014, **247**, 703-711.

14. G. Kalimuldina and I. Taniguchi, *J. Power Sources*, 2016, **331**, 258-266.

15. K. Jiang, Z. Chen and X. Meng, *ChemElectroChem*, 2019, **6**, 2825-2840.

16. J.-S. Chung and H.-J. Sohn, *J. Power Sources*, 2002, **108**, 226-231.

17. H. Wu, T. Li, H. Li, D. Zhang and F. Xu, *Mater. Lett.*, 2020, **262**, 127181.

18. W. Lou, M. Chen, X. Wang and W. Liu, *J. Phys. Chem. C*, 2007, **111**, 9658-9663.

19. O. Elimelech, J. Liu, A. M. Plonka, A. I. Frenkel and U. Banin, *Angew. Chem.*, 2017, **129**, 10471-10476.

20.   A. T. Sheardy, D. M. Arvapalli and J. Wei, *Nanoscale Adv.*, 2020, **2**, 1054-1058.

21.   S. Gorai, D. Ganguli and S. Chaudhuri, *Cryst. Growth Des.*, 2005, **5**, 875-877.

22.   S. Yadav, K. Shrivas and P. Bajpai, *J. Alloys Compd*, 2019, **772**, 579-592.

23.   S. Yadav and P. Bajpai, *Nano-Struct. Nano-Objects*, 2017, **10**, 151-158.

24.   C. H. Van Oversteeg, F. E. Oropeza, J. P. Hofmann, E. J. Hensen, P. E. De Jongh and C. de Mello Donega, *Chem. Mater.*, 2018, **31**, 541-552.

25.   J. Li, T. Jiu, G.-H. Tao, G. Wang, C. Sun, P. Li, J. Fang and L. He, *J. Colloid Interface Sci.*, 2014, **419**, 142-147.

26.   M. Jain, D. G. Babar and S. S. Garje, *Appl. Nanosci.*, 2019, **9**, 353-367.

27.   L. Liu, B. Zhou, L. Deng, W. Fu, J. Zhang, M. Wu, W. Zhang, B. Zou and H. Zhong, *J. Phys. Chem. C*, 2014, **118**, 26964-26972.

28.   M. Lee, J. Yang, H. Lee, J. I. Lee, A. R. Koirala, J. Park, H. Jo, S. Kim, H. Park and J. Kwak, *ACS Appl. Mater. Interfaces*, 2021, **13**, 26330-26338.

29.   Y. Zhao, H. Pan, Y. Lou, X. Qiu, J. Zhu and C. Burda, *J. Am. Chem. Soc.*, 2009, **131**, 4253-4261.

30.   J. M. Luther, M. Law, Q. Song, C. L. Perkins, M. C. Beard and A. J. Nozik, *ACS Nano*, 2008, **2**, 271-280.

31.   H. Zhang, J. Jang, W. Liu and D. V. Talapin, *ACS Nano*, 2014, **8**, 7359-7369.

32.   J. Lee, Y. Gim, J. Yang, H. Jo, J. Han, H. Lee, D. H. Kim, W. Huh, J. H. Cho and M. S. Kang, *J. Phys. Chem. C*, 2017, **121**, 5436-5443.

33.   A. Nag, M. V. Kovalenko, J.-S. Lee, W. Liu, B. Spokoyny and D. V. Talapin, *J. Am. Chem. Soc.*, 2011, **133**, 10612-10620.

34.   N. Y. Shim, D. A. Bernards, D. J. Macaya, J. A. DeFranco, M. Nikolou, R. M. Owens and G. G. Malliaras, *Sens.*, 2009, **9**, 9896-9902.

35.   S. Dong, B. Wang and B. Liu, *Biosens. Bioelectron*, 1992, **7**, 215-222.

36.   J. Kardos, L. Héja, Á. Simon, I. Jablonkai, R. Kovács and K. Jemnitz, *Cell Commun. Signal.*, 2018, **16**, 1-22.

37.   J. Brugger, B. Etschmann, W. Liu, D. Testemale, J.-L. Hazemann, H. Emerich, W. Van Beek and O. Proux, *Geochim. Cosmochim. Acta*, 2007, **71**, 4920-4941.

38.   K. Shakeela, A. S. Dithya, C. J. Rao and G. R. Rao, *J. Chem. Sci.*, 2015, **127**, 133-140.

39.   D. Shen, K. Steinberg and R. Akolkar, *J. Electrochem. Soc.*, 2018, **165**, E808.

40.   K. He, Z. Yao, S. Hwang, N. Li, K. Sun, H. Gan, Y. Du, H. Zhang, C. Wolverton and D. Su, *Nano Lett.*, 2017, **17**, 5726-5733.

41.   J. S. Nam, J.-H. Lee, S. M. Hwang and Y.-J. Kim, *J. Mater. Chem. A*, 2019, **7**, 11699-

11708.

42.   R. R. Gagne, C. A. Koval and G. C. Lisensky, *Inorg*, 1980, **19**, 2854-2855.

43.   H. Singh, S. Kumar and P. K. Sharma, *Appl. Surf. Sci.*, 2023, **612**, 155831.